Proceedings of the 5th IEEE
International Symposium on Assembly and Task Planning
Besançon, France • July 10-11, 2003

Contact and Force Control in Microassembly

Yantao Shen† Ning Xi† Wen Jung Li*

†Dept. of Electrical and Computer Engr.
Michigan State University
East Lansing, MI
USA

*Dept. of Automation and Computer-Aided Engr.
The Chinese University of Hong Kong
Shatin, N. T., Hong Kong SAR
China

Abstract

This paper aims at advancing micromanipulation technology with in-situ PVDF piezoelectric force sensing and control during microassembly and packaging process. To allow close monitoring of magnitude and direction of forces (surface, friction, and assembly force) acting on micro devices during manipulation, the polyvinylidene fluoride (PVDF) is used to fabricate highly sensitive 1-D and 2-D force sensors for assembly of micro devices. By using the designed force sensors with the effective signal processing techniques, the contact force/impact signal can be obtained desirably so that it greatly improves the reliability of force regulation in microassembly. Moreover, based on a new sensor-referenced control method, the force control had been implemented by employing a micromanipulator system equipped with the force sensor and its results verify the effectiveness of sensor model as well as the performance of force feedback and control system. Ultimately the technology will provide a critical and major step towards the development of automated manufacturing processes for batch assembly of micro devices.

1 Introduction

Manufacturing processes which are capable of quickly and cheaply assembling MEMS devices have not been developed, partly because, at the micro-scale, structures are fragile and easily breakable. They typically break at the micro-Newton (μN) force range– a range that cannot be felt by a human operator assembling microstructure with tweezers and microscopes, and is not reliably measurable by the existing force sensors during assembly. As a result, it is extremely difficult to manipulate parts for assembly at that scale. Moreover, this situation decreases overall yield and driving up cost of MEMS [1].

For these reasons, research into automating the microassembly process has firstly focused on force sensing techniques [2]. Currently, there exist some developing sensing mechanisms commonly used in sensing contact force in microassembly such as strain gauges, piezoresistive effect, piezomagnetic effect, capacitive sensors [2], optical techniques [3] and piezoelectric effect (PZT-based) [4]. For strain gauges, piezoresistive effect, piezomagnetic effect and capacitive sensors, their resolutions are in the range of sub-mN or mN. Although the optical techniques have high resolution in range of nano-Newton (nN), to compare to the other methods, the optical techniques are more expensive. Here, more suitably, the resolution of force sensor based on piezoelectric effect is in the range of μN generally.

Besides force sensing, another key issue in microassembly is the micro force feedback and control. A low level proportional impact force control scheme using nano scale optical beam deflection force feedback, is implemented to reduce the large impact effects [6]. In [7], Tanikawa et al. report that the high success rate of the grasp task can not be obtained with a developed stiffness-like-force-control scheme. By investigations, it is reasonable to state that a very few successful micro contact/impact force controllers have been reported. However, in a micro environment, the impact/contact forces become even more important because the mass of the manipulated object and manipulator itself become relatively small compared to the velocity. Therefore, it is rather necessary to develop a robust and intelligent contact/impact force controller to achieve a reliable and efficient micro assembly.

Traditionally, the task of phase transition or contact/impact control can be divided into the following three operation modes: free motion mode, phase transition mode (or impact mode), and contact-motion mode. Large impact forces and possible bouncing may occur during the impact mode. Control of phase transition has been a research subject for several years and various schemes have been proposed. Basically, the existing schemes can be divided into two categories. The first category is impedance control [8]. It provides a stable and unified control structure for the

0-7803-7770-2/03/$17.00 ©2003 IEEE

phase transition. The problem with the impedance control is that, after contact has been established, the output force cannot be regulated unless the exact environmental model was known and was integrated into the motion plan. In contrast to impedance control, several discontinuous control schemes have been proposed, typically in [9]. The major result is that the output force can be regulated after the impact. But this may not be true if bouncing occurs during the impact. Back to the microassembly in micro environment, the impact/contact force control becomes more difficult. Partly because, the impact/contact force is too small to detect easily and the unknown disturbances exist largely during the control process.

The objective of this paper is to pursue the most feasible and versatile solution in the impact/contact force control for microassembly, which is based on the use of PVDF-based force sensor as a sensing device during the process of microassembly. With respect to PZT-based piezoelectric force sensors, the piezoelectric polymer PVDF is a more ideal sensing device because of its low-Q response, ease of use, compliance and high sensitivity. In accordance with the piezoelectric effect and the mechanics of material for bending cantilever beam, we developed both the models and the structures of 1-D and 2-D PVDF high sensitivity force sensors with the resolution in range of sub-μN. By equipping the force sensors at the front of micromanipulator, the micro force acting at the sensor tip during manipulation can be detected desirably and then be fed back to the control system on-line. Furthermore, based on a new sensor-reference control method, the experiments on micro impact/contact force control and regulation during the impact mode and the contact-motion mode have been conducted. The results demonstrate the performance of the developed force sensing and control system. That is, the force sensing and control system can be used for automated microassembly such as reliable assembly of the micro mirrors, and impact/contact force can be regulated desirably to maintain a safety margin during the assembly. The resulting higher and faster yield will make batch fabrication and assembly of micro devices a reality.

2 Force Sensing Model

2.1 1-D Sensor Model

As shown in Figure 1, a 1-D PVDF sensor model is developed. Based on the piezoelectric effect, the unit polarization factor of the PVDF film $D_3(x,t)$ can be expressed as: (without considering the inverse piezoelectric affection and pyroelectric effects)

$$D_3(x,t) = d_{31}\sigma(x,t) + \varepsilon_{33}^T E_3(t) \qquad (1)$$

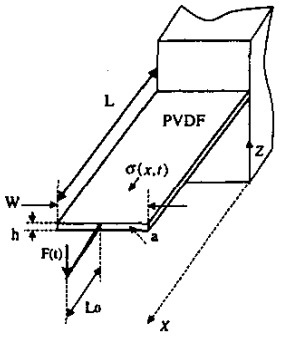

Figure 1: 1-D sensor.

where d_{31} is the piezoelectrical coefficient of the PVDF film; $\sigma(x,t)$ is unit stress; ε_{33}^T is the dielectrical factor of the PVDF film; $E_3(t)$ represents the electrical field of the PVDF film.

The total charge $Q(t)$ across the PVDF surfaces area A $(L \times W)$ is

$$Q(t) = \int D_3(x,t)dA. \qquad (2)$$

The unit stress on PVDF can be calculated as

$$\sigma(x,t) = \frac{F(t)(L-x)\frac{h}{2}}{I} + \frac{F(t)L_0\frac{h}{2}}{I} \qquad (3)$$

where the neutral axis of the bending deflection of beam is assumed to pass through the centroid of the cross-sectional area a. $F(t)$ is the contact force acting at the sensor tip. I denotes inertial moment of cross-sectional area a $(W \times h)$. L_0 is the length of the sensor tip. Since the generation of charge is the same along the width of the PVDF,

$$\begin{aligned} Q(t) &= \int_0^L (d_{31}\sigma(x,t) + \varepsilon_{33}^T E_3(t))W dx \\ &= \frac{d_{31}Ah(L_0 + \frac{L}{2})}{2I}F(t) + \varepsilon_{33}^T E_3(t)A. \end{aligned} \qquad (4)$$

By piezoelectrical effect, note that if no charge builds up by the external force, the $E_3(t)$ will be zero. Then, by an equivalent circuit of model of parallel a resistor R_P and a capacitor C_P for the PVDF film. The output voltage $V(t)$ across the PVDF film, can be described by

$$\frac{V(t)}{R_P} + \dot{V}(t)C_P = \frac{dQ}{dt}. \qquad (5)$$

Since the electrical field $E_3(t) = -\frac{dV(t)}{dh}$, therefore $E_3(t) = -\frac{V(t)}{h}$ for uniform electric field over the very small hight h. Thus

$$\dot{E}_3(t) = -\frac{\dot{V}(t)}{h}, \qquad (6)$$

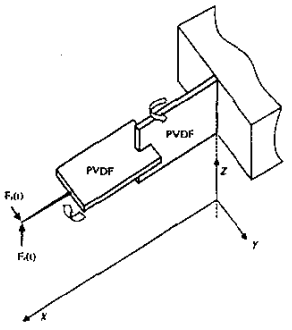

Figure 2: 2-D force sensor

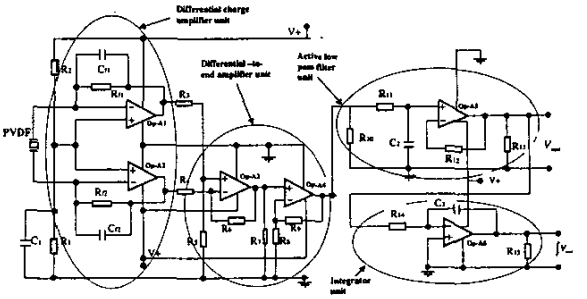

Figure 3: Electronic circuit.

and then the relationship between the output voltage and the contact force can be obtained as

$$V(t) + \lambda \dot{V}(t) = B\dot{F}(t) \tag{7}$$

where $C_P = \frac{\varepsilon_{33}^T A}{h}$ is the capacitance of the PVDF film; $\lambda = 2R_P C_P$ and $B = \frac{R_P A d_{31} h(L_0 + \frac{L}{2})}{2I}$ are constants.

By the Laplace transformation, the electrical transfer function of the PVDF sensor is given as:

$$T(s) = \frac{V(s)}{F(s)} = \frac{B}{\lambda} \frac{\lambda s}{1 + \lambda s}. \tag{8}$$

Based on the 1-D model, a design for 2-D PVDF force sensor has been proposed as shown in Figure 2. In each direction, a 1-piece beam is used to detect the force. It can also be seen that this structure provides a decoupled force measurement in the Y and Z directions. The decoupled output voltages and forces can be described as

$$\begin{aligned} V(t) + \lambda_Z \dot{V}(t) &= B_Z \dot{F}_Z(t) \\ V(t) + \lambda_Y \dot{V}(t) &= B_Y \dot{F}_Y(t). \end{aligned} \tag{9}$$

Note that, to improve the rigidity of the structure and, at the same time, to increase the sensitivity of the force sensing in that direction, the 2-D sensor can also be designed by virtue of a parallel beam structure.

2.2 The Electronic Circuit

Preprocessing of sensed data is critical by the circuit for two reasons: (i) remove any noise, (ii) amplify and extract the desired signal which is in this case the force. The simplified diagram of the developed circuit is shown in Figure 3.

In this circuit, a differential charge amplifier is designed for PVDF force sensors firstly. The differential charge amplifier is based on the chopper stabilized operational amplifier TC7650C with a high input impedance $10^{12}\Omega$ and low bias current $1.5pA$. Following the charge amplifier, a differential-to-single-ended amplifier is added. The total differential topology can reduce the common mode noises more effectively. To reject the existing high frequency noises, an active low pass filter with the cutoff frequency $160Hz$ is used before the voltage output. The integration of the output voltage by time can also be achieved by an integrator unit in the circuit. In addition, the reduction of RFI (Radio Frequency Interference) and EMI (Electromagnetic Interference) have been accounted for in the circuit by the related filtering and shielding.

2.3 System Transfer Function

By considering the whole circuit, the transfer function is approximated by

$$\begin{aligned} \frac{V_{out}(s)}{V(s)} &= -\frac{2R_f C_P s}{1 + R_f C_f s} \times -K_c \times \frac{1}{1 + \tau_1 s} \\ &\doteq \frac{2K_c C_P}{C_f} \times \frac{1}{1 + \tau_1 s} \end{aligned} \tag{10}$$

where $R_{f1} = R_{f2} = R_f$. $C_{f1} = C_{f2} = C_f$. K_c is the gain of the differential-to-single-ended amplifier. R_f is chosen as a very large value resistor. τ_1 is a rather small time constant of the designed active low pass filter.

Finally, from eqns (8) and (10), the global transfer function of the sensor system is

$$GT(s) = \frac{V_{out}(s)}{F(s)} \doteq \frac{K_c B}{R_P C_f} \frac{\lambda s}{(1 + \lambda s)(1 + \tau_1 s)}. \tag{11}$$

The function is a bandpass type filter. Since τ_1 is very small in the circuit, eqn(11) can be rewritten as

$$GT(s) = \frac{V_{out}(s)}{F(s)} \doteq \frac{K_c B}{R_P C_f} \frac{\lambda s}{(1 + \lambda s)}. \tag{12}$$

By filtering this signal over an appropriate pass band and then integrating with respect to time, this generates the

force rate and the force, over this pass band, respectively. In a case, the force is obtained by measuring the output voltage of sensor system when the initial values $F(t_0)$ and $V_{out}(t_0)$ are known.

$$F(t) - F(t_0) = \frac{C_f}{2K_c B C_P}[\lambda(V_{out}(t) - V_{out}(t_0)) + \int_{t_0}^{t} V_{out}(t)dt] \quad (13)$$

3 Contact Force Control

In this section, a new sensor-referenced control method for impact/contact control and force regulation of a micro manipulator will be proposed [10]. It utilizes the positive acceleration feedback together with a switching control strategy to achieve a stable impact/contact control and force regulation in micromanipulation/microassembly.

3.1 Feedback Linearization

Traditionally, the dynamic equation for a micromanipulator with n degrees of freedom is given by

$$\begin{aligned} H(q)\ddot{q} + C(q,\dot{q}) + G(q) &= \tau - J^T(q)F \\ y &= h(q) \end{aligned} \quad (14)$$

where $h(q)$ is the forward kinematics; y is the output positions and orientation in the task space, F is the output force in the task space. Based on the equation (14), introducing the nonlinear feedback control law:

$$\tau = H(q)J^{\#}(q)(v - \dot{J}(q)\dot{q}) + C(q,\dot{q}) + G(q) + J^T(q)F \quad (15)$$

where $J^{\#}(q)$ is the pseudo inverse of the Jacobian matrix. As a result, the dynamics of the micromanipulator can be linearized and decoupled as

$$\begin{aligned} \ddot{y}_u &= v_u \\ \ddot{y}_c &= v_c \end{aligned} \quad (16)$$

where y_u represents the output positions and orientation in the unconstrained directions; and y_c represents the output positions and orientation in the constrained directions. Let v_u, v_c represent the auxiliary input vectors. Therefore, the motion of the manipulator can be controlled independently for each direction.

3.2 Force-Referenced Controller

During the phase transition mode, in the constrained directions, the position control is used before the detection of impact, that is

$$v_c = \ddot{y}_c^d + k_{vc}(\dot{y}_c^d - \dot{y}_c) + k_{pc}(y_c^d - y_c), \qquad t < t_{sw} \quad (17)$$

where k_{vc} and k_{pc} represent derivative gain and proportional gain, respectively. y_c^d is the desired position. t_{sw} represents the time of the detection of impact. Once the impact is detected, the controller will switch from position control to force control in the constrained direction. The switching logic is given as follows.

$$\begin{aligned} &\text{If } U = \{\{\dot{y}_c(t_{sw}) > 0 \cap F_c = F_{sw}\} \cup F_c < F_{sw}\} \\ &\qquad \text{then position control} \\ &\text{If } C = \{\{\dot{y}_c(t_{sw}) \le 0 \cap F_c = F_{sw}\} \cup F_c > F_{sw}\} \\ &\qquad \text{then force control} \end{aligned} \quad (18)$$

where F_{sw} is minimum detectable force. The position $y_c(t_{sw})$ corresponding to F_{sw} is unknown, but can be recorded on line to serve as the desired position for position control. To track the desired force during the impact in constrained directions, at the same time, to avoid a large impulsive force after impact, we implement the following force controller

$$v_c = k\ddot{y}_c + k_d\dot{y}_c + k_f(F_c^d - F_c) + k_I \int_{t_{sw}}^{t} (F_c^d - F_c)dt, \qquad t \ge t_{sw} \quad (19)$$

where $F_c^d, F_c, k_d, k_f, k_I$ represent the desired force, the actual force response, and the force gains in the constrained directions. The coefficient k is chosen to be less than one and is to use for reducing the affection from the noises induced by the acceleration. It is noticed that the measurement of acceleration is required. It could be difficult to obtain a real-time acceleration measurement. Therefore, we propose to use the prior calculated value of the acceleration based on equation (14). This method has been used in another applications [10] with satisfactory results. In the contact-motion mode, position control is used for the unconstrained directions only, i.e.,

$$v_u = \ddot{y}_u^d + k_{vu}(\dot{y}_u^d - \dot{y}_u) + k_{pu}(y_u^d - y_u). \quad (20)$$

At the same time, the force regulation can be realized in the constrained directions.

4 Experiment

4.1 Set-up

The experiments was conducted on a micro robotic system shown in Figure 4. The micro robotic system mainly consists of a SIGNATONE Computer Aided Probe Station and a Mitutoyo FS60 optical microscope system. The micro robot is controlled by a PC-based control system. The control system is an open platform which can

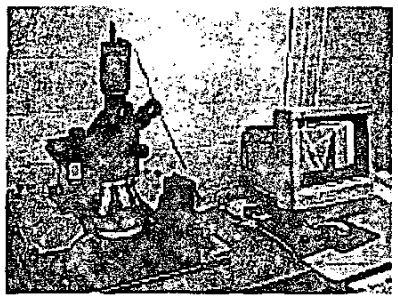

Figure 4: A micro robotic system at MSU.

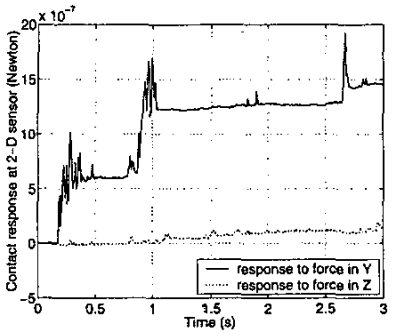

Figure 5: 2-D sensor responses when force exerting along Y .

easily integrate with the developed PVDF force sensing system. The PVDF force sensor (1-D) has the following dimensions and parameters: $L0 = 0.0225m; L = 0.0192m; w = 0.0102m$; $h = 28\mu m$ (PVDF film); $Rp = 1.93 \times 10^{12}\Omega; Cp = 0.90 \times 10^{-9}F; E = 2 \times 10^{9}N/m^2$. The sensor system had been calibrated with a resolution in range of sub-μN and sensitivity $6.0245V/\mu$N.

The force signal processed by the designed circuit are transferred to micro robotic system via a multifunction analog/digital input/output board AX5411H installed in another PC. There exists a communication between the PC and micro robotic system. The sampling frequency of AX5411H is 1KHz in the experiment. The maximum encoder frequency of micromanipulator motor is 8×10^6 counts/s with 14-bit DAC resolution. The loop time of the force sensing and control system is about 2ms. To reduce vibrations from the environment, an active vibration isolated table was used during the experiment.

4.2 Force Sensing

An experiment on the continual contact-stop action has been conducted to verify the sensing and self-decoupling of the 2-D force sensor (referring to Fig.2). The 2-D force signals detected are plotted in Figure 5. The result verifies the performance of sensing and self-decoupling of the 2-D sensor.

4.3 Contact Force Control

Continually, using the 1-D sensor to contact a planar glass surface, the contact force control experiments are implemented. Figure 6 plots one of the force control results in which the desired force F_c^d of the contact tip is set as 9.4×10^{-6} Newton. The gains are $k = 0.7, k_d = 0.5, k_f = 25, k_I = 25$. In this experiment, the path is down from a initial point in free space to a contact point on the constrained glass surface(along -Z direction). In Figure 7, it shows another experiment with the setting of the desired contact force $F_c^d = 1.88 \times 10^{-6}$ Newton, the gains are $k = 0.7, k_d = 1, k_f = 25, k_I = 25$. Differing from the above experiment, the path consists of two segments: firstly, the sensor tip is down from a initial point in free space to a contact point on the constrained glass surface (along -Z direction), after a period of force regulation, starting from 0.76s, the sensor tip is controlled to move a straight line along Y direction on the constrained glass surface from the contact point (note that the Y and Z directions are perpendicular each other), at the same time, the contact force is still regulated in the contact direction (Z direction). The two experimental results have shown both on the detection of the contact and the contact-motion mode, the force controls make the force error go to zero asymptotically with a small peak impact force and bouncing. They both confirm the performance that the developed system can effectively regulate micro contact force to maintain safety margins during microassembly.

5 Conclusions

In this paper, based on using polyvinylidene fluoride (PVDF) to fabricate highly sensitive 1-D and 2-D force sensors, we develop a micro force feedback and control system for microassembly. By the developed system, the impact/contact force can be effectively regulated so as to maintain safety margins and to greatly improve reliability and yield during microassembly. Experimental results verified the performance of the force sensing and control scheme. Ultimately the technology will provide a major step to make batch fabrication and assembly of micro devices a reality.

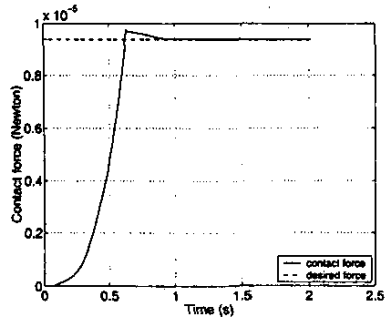

(a) Contact force

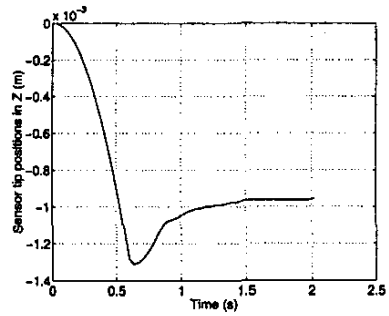

(b) Tip positions in Z

Figure 6: Contact force control I

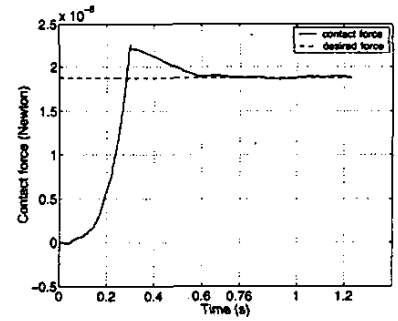

(a) Contact force

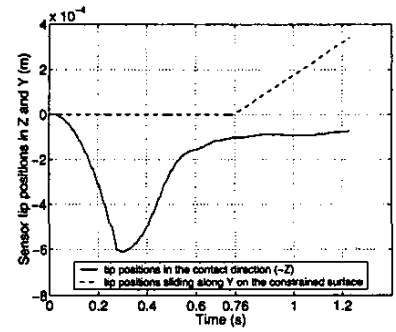

(b) Tip positions in Z and Y

Figure 7: Contact force control II

References

[1] S. K. Koelemijer Chollet, L. Benmayor, J.-M. Uehlinger and J. Jacot, *Cost Effective Micro-System Assembly Automation*, Emerging Technologies and Factory Automation. Proceedings. ETFA '99. Vol. 1, pp. 359-366, 1999.

[2] S. Fahlbush and S. Fatikow, *Micro Force Sensing in a Micro Robotic System*, ICRA 2001, pp. 3435-3440, 2001.

[3] B. Nelson, Y. Zhou and B. Vikramaditya, *Sensor-based micro-assembly of hybrid MEMS devices*, IEEE Control System Magazine. Vol. 18, no.6 pp. 35-45, 1998.

[4] C. Lee, T. Itoh and R. Suga, *Micromachined Piezoelectric Force Sensors Based on PZT Thin Films*, IEEE Transactions on Ultrasonics, Ferroelectrics, and Frequency Control. Vol. 43, no. 4, pp. 553-559, 1996.

[5] C. K. M. Fung, I. Elhajj, W. J. Li, and N. Xi *A 2-D PVDF Force Sensing System for Micro-manipulation and Micro-assembly*, Proc. of the IEEE International Conference on Robotics and Automation, pp. 1489-1494, 2002

[6] Y. Zhou, B. J. Nelson and B. Vikramaditya. *Fusing Force and Vision Feedback for Micromanpulation* Proceeding of IEEE International Conference Robotics and Automation, pp. 1220-1225, 1998.

[7] T. Tanikawa, M. Kawai, N. Koyachi, T. Arai, T. Ide, S. Kaneko, R. Ohta and T. Hirose. *Force Control System for Autonomous Micro Manipulation*, Proceeding of IEEE International Conference Robotics and Automation, pp. 610-615, 2001.

[8] N. Hogan, *Impedance Control: An Approach to Manipulation: Part I - Theory and Part II - Implementation*, J. Dynamical Systems, Meas. Control, Vol. 107, pp. 1-16, March 1985.

[9] J. Hyde, M. Cutkosky, *Contact Transition Control: An Experimental Study*, Proceedings of International Conference on Robotics and Automation, pp. 363-368, 1993.

[10] T. J. Tarn, Y. Y. Wu, N. Xi, and A. Isidori, *Force Regulation and Contact Transition Control*, IEEE Control Systems, pp. 32-40, February 1996.